

Modeling bottom roughness in the presence of wave-generated ripples

Richard Styles

Marine Science Program and Department of Geological Sciences, University of South Carolina
Columbia, South Carolina, USA

Scott M. Glenn

Institute of Marine and Coastal Sciences, Rutgers University, New Brunswick, New Jersey, USA

Received 8 March 2001; revised 19 December 2001; accepted 15 January 2002; published 23 August 2002.

[1] Near-bottom wave, current and microtopography measurements have been obtained at the LEO-15 site off the southern coast of New Jersey. The measurements are used in conjunction with a recently calibrated continental shelf bottom boundary layer model to refine estimates of bottom roughness for a rippled bed under combined wave and current flows. In the presence of nearly two-dimensional wave-generated ripples, application of the *Grant and Madsen* [1979] type bottom boundary layer model produces estimates of the bottom roughness felt by the current that are several times greater than established formulations for rippled beds under waves. Modifying one of the primary length scales in the eddy viscosity profiles returns estimates that are more consistent with the wave roughness results. Application of the roughness model in conjunction with a refined empirical ripple geometry model produces highly accurate estimates of measured shear velocities and apparent roughnesses during a moderate storm. The demonstrated accuracy of this simple combined roughness and ripple geometry formulation reveals its utility when considering applications of coupled bottom boundary layer–shelf circulation models.

INDEX TERMS: 4211 Oceanography: General: Benthic boundary layers; 4546 Oceanography: Physical: Nearshore processes; 4558 Oceanography: Physical: Sediment transport; 4568 Oceanography: Physical: Turbulence, diffusion, and mixing processes; *KEYWORDS:* bottom roughness, bed form prediction, bottom stress

1. Introduction

[2] The length scales that define the bed roughness in turbulent flows are fundamental parameters of boundary layer research. The physical roughness, k_b , is proportional to the hydraulic roughness, which scales the vertical coordinate within the constant stress layer [*Tennekes and Lumley*, 1972; *Hinze*, 1975] and is often used to define the location of boundary fluxes of momentum and suspended sediment concentrations in models [e.g., *Smith*, 1977; *Smith and McLean*, 1977; *Wiberg and Smith*, 1983; *Glenn and Grant*, 1987; *Nielsen*, 1992]. On wave-dominated sandy continental shelves, the largest roughness conditions are arguably associated with wave-generated bedforms. Much of what is known about the roughness and geometrical characteristics of wave-generated sand ripples has come from laboratory studies [e.g., *Carstens et al.*, 1969; *Lofquist*, 1986; *Rankin and Hires*, 2000]. *Grant and Madsen* [1982] found that k_b for equilibrium conditions, in which ripple height tends to grow with increasing wave orbital diameter and ripple steepness is nearly constant, was well represented as a constant times the product of the ripple height (η) and ripple steepness (η/λ), where λ is the ripple wavelength. On the basis of the sand ripple data of *Carstens et al.* [1969] and the fixed bedform data of *Bagnold* [1946], they found that the simple formula,

$k_b = 27.7\eta(\eta/\lambda)$, produced good estimates of the wave friction factor when used in conjunction with their wave boundary layer model to compute the maximum wave stress. *Nielsen* [1992] obtained a similar result based on the water tunnel data of *Carstens et al.* [1969] and *Lofquist* [1986], but with a significantly lower value for the proportionality factor, i.e., $k_b = 8\eta(\eta/\lambda)$. Because ripple steepness has a nearly constant value of about 0.15 under equilibrium conditions, k_b can be expressed uniquely as a function of ripple height, $k_b = (1 - 4)\eta$. This simple formula has also been confirmed through laboratory studies of oscillatory flow over equilibrium sand ripples [*Wikramanayake and Madsen*, 1991; *Rankin and Hires*, 2000].

[3] Given the strong correlation between ripple geometry and bottom roughness demonstrated in these laboratory studies, the above formulations are routinely applied to wave-dominated conditions in the field [*Drake and Cacchione*, 1992; *Drake et al.*, 1992; *Gross et al.*, 1992; *Xu and Wright*, 1995; *Li et al.*, 1996; *Li and Amos*, 1998; *Williams et al.*, 1999]. Previous studies designed to provide an experimental basis for either the *Grant and Madsen* [1982] or *Nielsen* [1992] roughness models [*Drake et al.*, 1992; *Xu and Wright*, 1995; *Li and Amos*, 1998], have relied on the original *Grant and Madsen* [1979, 1986] combined flow model to compute the shear stress components. If the ambient flow conditions remained fixed, the bottom stress will be a function of the bed roughness. Because the bottom roughness calculation depends on the

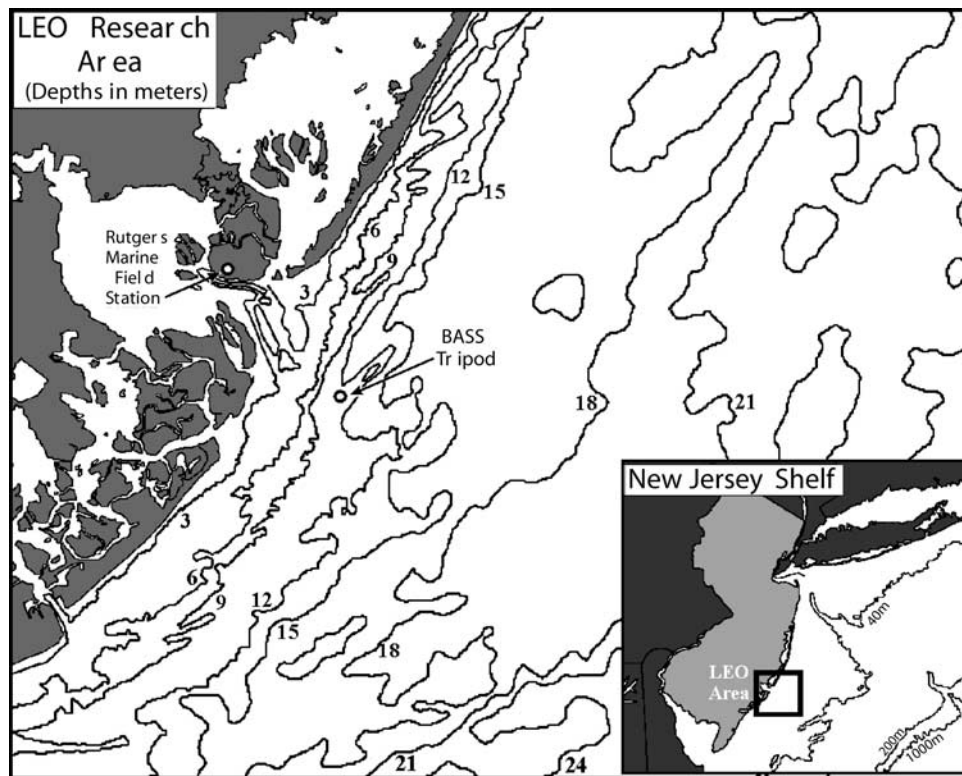


Figure 1. The LEO-15 research site located off of the southern coast of New Jersey. Inset: regional coastline. Area of detail: tripod location.

particular combined flow model to estimate the shear stress, any extrapolation of the *Grant and Madsen* [1982] or *Nielsen* [1992] bottom roughness formulations must be similarly calibrated when used in conjunction with other bottom boundary layer models. *Madsen and Wikramanayake* [1991] showed that a modification to the *Grant and Madsen* [1979] discontinuous eddy viscosity profile produced estimates of current profiles that better agreed with flume observations and the numerical combined flow model of *Davies et al.* [1988]. *Styles and Glenn* [2002] recently modified the *Madsen and Wikramanayake* [1991] model to include very rough conditions under waves and combined flows. The *Styles and Glenn* [2002] version was calibrated with bottom roughness and wave stress measurements obtained in a flume with co-directional waves and currents [*Mathisen and Madsen*, 1996]. This model has not been field calibrated to determine an optimal bed roughness formulation for very rough beds.

[4] The primary purpose of this paper is to combine historical data sets, recent field data, and a newer version of the *Grant and Madsen* [1979] combined flow model to further investigate the relationship between bottom roughness and the geometric characteristics of nearly 2-D wave-generated ripples. The following section describes a field experiment conducted offshore of Tuckerton, New Jersey, in which high-quality near-bottom currents, waves and microtopography measurements were acquired. Section 3 describes the data selection and analysis, and is followed in section 4 by an empirical evaluation of the proportionality constant relating k_b to ripple geometry. Because bottom roughness is known to be linked to ripple geometry, section 5 introduces

a modification of a simple model [*Wikramanayake and Madsen*, 1991] to predict ripple height and length primarily as a function of the wave excursion amplitude and wave orbital velocity. This is followed in section 6 by an application of the present combined bottom roughness/ripple geometry model to predict the shear velocity and apparent roughness during a storm. The major results of this study are summarized in section 7.

2. Study Site and Instrumentation

[5] All field data for this study were collected at the LEO-15 (Long-term Ecosystem Observatory) site (Figure 1) located approximately 10 km off of the southern coast of New Jersey [*von Alt and Grassle*, 1992; *Glenn et al.*, 2000]. In August and September of 1994 and 1995, benthic boundary layer tripods were deployed for approximately 3 and 6 weeks, respectively, to study near-bottom flow and sediment transport at this sandy continental shelf site. The water depth at the study site is approximately 12 m and the bottom consists of a mixture of mostly quartz sand with a median grain diameter of 0.04 cm [*Traykovski et al.*, 1999]. The flow in the bottom boundary layer was measured with a Benthic Acoustic Stress Sensor (BASS) tower [*Williams et al.*, 1987]. In 1994 the BASS was deployed on a small tripod. In 1995 it was placed on a larger tripod that also included acoustic sensors to measure suspended sediment concentration profiles and bedform geometry [*Traykovski et al.*, 1999]. The BASS tower accommodated an array of 4 current meters with center heights placed at 55, 91, 125 and 241 cm above the bottom during the 1994 deployment and

at 45, 80, 165 and 250 cm above the bottom during the 1995 deployment. A pressure sensor was positioned at 191 cm between the third and fourth BASS sensor during the 1994 deployment and at 416 cm above the bottom during the 1995 deployment. A temperature and a salinity probe were also connected to the BASS data logger and were placed at approximately the same height as the pressure sensor. The current, pressure, temperature and salinity sensors were synchronized and programmed to sample at 4 Hz for a 15-minute burst each hour.

[6] During the 1995 deployment, bedform geometry was primarily measured with a Sector Scanning Sonar (SSS) [Hay and Wilson, 1994; Traykovski et al., 1999]. The unit was mounted approximately 1 m away from the BASS tower looking downwards and acquired a single seafloor image within a circular area of approximately 3 m radius every 30 minutes. By combining the SSS images with a narrow beam acoustic profiler that could map the temporal evolution of the bottom, Traykovski et al. [1999] were able to generate an accurate time series of ripple height and length. Therefore, the SSS provides direct measurements of the dominant roughness elements concurrent with the BASS current, wave and stress measurements almost continuously for a period of about 6 weeks.

3. Calculation of Model Input Parameters

[7] A model to describe the bottom roughness must relate the geometrical properties of the dominant roughness elements to the turbulent-induced frictional dissipation (bed shear stress) associated with the flow. For combined flows, bottom boundary layer models (BBLMs) [e.g., Smith, 1977; Grant and Madsen, 1979] make it possible to evaluate the stress components associated with the waves and currents in terms of the more easily measured near-bottom horizontal flow field. In the present application, the flow components needed to drive the BBLM include the current magnitude, u_r , at a known height above the bottom, z_r , the angle between the wave and current, φ_{cw} , the near-bed excursion amplitude of the wave, A_b , and the near-bed orbital velocity, u_b .

[8] Current data needed to compute u_r and φ_{cw} were obtained from the highest BASS sensor in 1994 and the lowest sensor in 1995. In 1994, the highest sensor was positioned on top of the tripod, where flow interference due to the tripod structure was minimized. In 1995, all sensors were mounted below the apex of the tripod, with the lowest sensor positioned the furthest away from any of the legs. The lowest sensor was least likely to experience flow interference from the tripod during periods when one of the legs was directly upstream of the BASS tower. The coordinate system was aligned so that the x axis was oriented offshore toward the east and the y axis was oriented alongshore toward the north. The height of the sensors defined z_r and the mean current was obtained by averaging the current record over each 15-minute burst sampling period.

[9] For the wave, each 15 minute burst pressure record was fast Fourier transformed to produce the wave pressure spectrum. Transfer functions from linear wave theory then were used to convert the pressure spectrum to the near-bottom orbital velocity spectrum, $S_{u_b}(\omega)$, which is a function of the wave radian frequency, ω . Given the velocity

spectrum, u_b was calculated in terms of the equivalent wave defined by Madsen et al. [1988], i.e.,

$$u_{beq} \equiv \sqrt{2 \int_0^{\infty} S_{u_b}(\omega) d\omega}. \quad (1)$$

Similarly, the equivalent wave radian frequency was given by

$$\omega_{eq} = \frac{\int_0^{\infty} \omega S_{u_b}(\omega) d\omega}{\int_0^{\infty} S_{u_b}(\omega) d\omega} \quad (2)$$

so that A_{beq} was calculated as u_{beq}/ω_{eq} [Madsen, 1994]. The wave direction was determined as the angle between the x axis and maximum horizontal velocity variance from the sensors described in the previous paragraph.

[10] Although the total boundary shear stress was not measured, indirect estimates of the time average shear stress and apparent roughness were obtained by fitting log profiles to the BASS current measurements. The model equation is the classic law-of-the-wall for a combined wave and current flow,

$$U(z) = \frac{u_*^c}{\kappa} \ln\left(\frac{z}{z_{0c}}\right), \quad (3)$$

where u_*^c is the time average shear velocity associated with the current, κ is von Karmans constant (0.4) and z_{0c} is the apparent hydraulic roughness. Using well established statistical methods [Gross and Nowell, 1983; Gross et al., 1992], (3) is manipulated to produce a linear equation and a regression analysis is applied to calculate u_*^c and z_{0c} . Assuming Gaussian statistics, confidence limits based on the regression coefficient, R , are assigned to each burst estimate of these parameters [Gross and Nowell, 1983]. Other techniques to determine the bottom stress such as the inertial dissipation or the direct covariance method are generally unreliable in wave-dominated conditions for our sensor array configuration [Gross et al., 1994; Trowbridge, 1998]. As a result, stress estimates from these techniques are not pursued here.

[11] The purpose of this study is to calibrate a recently upgraded BBLM to be applied in the presence of a field of nearly 2-D wave-generated ripples. Because ripple formation and maintenance are coupled to sediment transport processes, existing 2-D ripple models generally apply only when the bed shear stress based on skin friction exceeds the minimum for the initiation of sediment motion [Nielsen, 1981; Grant and Madsen, 1982; Wiberg and Harris, 1994]. Observations of ripple migration and sediment resuspension during the 1995 deployment indicated that the waves were energetic enough to mobilize bed sediment almost continuously between about year day 240 and 255 [Traykovski et al., 1999]. Although sediment motion was observed during some bursts after this time period, biofouling began to significantly reduce the quality of the current measurements. Therefore, only data before year day 255 is considered.

[12] When bottom currents are fairly small (<5 cm/s [Gross *et al.*, 1992]) the shear-induced turbulent stresses may be too weak to generate a sufficiently thick constant stress layer to cover the vertical measurement range of our current sensor array. In the limit $\delta_c/z_0 \rightarrow \infty$, where δ_c is the height of the current boundary layer, similarity theory dictates that the approximation of logarithmic profile extends higher into the boundary layer than the approximation of constant stress [Blackadar and Tennekes, 1968]. For the present case, the boundary layer thickness is much greater than z_0 , so that the above argument applies. This implies that even if the constant stress layer lies somewhere below the measurement height of the BASS sensor array, there can exist a logarithmic region higher in the water column in which the shear stress and bottom roughness can be determined accurately from (3). Near-bed tidal currents at LEO-15 are generally less than about 5 cm/s so that stronger bottom currents are likely to occur in conjunction with wind or buoyancy forcing. Wind, wave and current conditions during the 1995 deployment are presented in Figure 2. Increases in bottom currents are generally well correlated with the low-passed filtered wind vectors. The equivalent bottom orbital velocity is greater than about 15 cm/s, but it never exceeds 30 cm/s. The lower limit represents the approximate threshold for initiation of motion based on the critical Shields parameter for the 0.04 cm grains found at LEO-15. On the basis of Bagnold [1956], Komar and Miller [1975], and Wilson's [1989] criteria for sheet flow, the upper velocity limit is still small enough so that the bottom stress based on skin friction for the wave never becomes strong enough to washout the ripples. As mentioned above, a defining characteristic of equilibrium ripples is that η/λ is a constant and nearly equal to a maximum and that λ increases in proportion to A_b . Traykovski *et al.* [1999] showed that during the majority of the chosen time period the bedforms were characteristic of equilibrium ripples. The hydrodynamic and bedform characteristics between year day 240 and 255 favor the simultaneous presence of a well developed constant stress layer and an equilibrium ripple field.

[13] Time averaged shear stress and apparent roughness are computed for each burst that indicated a depth-averaged current greater than 5 cm/s. To identify log profiles, we adopt the $Z = \tanh^{-1}(R)$ statistic used by Gross *et al.* [1992]. Taking the mean of Z for all bursts between year day 240 and 255 and inverting gives a minimum R^2 of 0.96 (62% error at the 95% level of significance). Because the constant stress layer argument is based on the assumption of unidirectional flow, each of these bursts is further checked to identify significant veering of the horizontal current as a function of depth [Madsen *et al.*, 1993]. Bursts that indicate a maximum veering angle between any 2 pairs of sensors greater than 10 degrees are rejected. The results of these calculations produce a total of 44 bursts for the calibration. The timing of the bursts with respect to the 15-day record is depicted in Figure 2c. Nearly all of the bursts are associated with strong alongshore currents but highly variable and much weaker cross-shore flows. The regression analysis has identified profiles that are consistent with a dominant bottom stress component in the alongshore momentum balance and an associated logarithmic velocity profile.

[14] Stable density stratification within the constant stress layer can distort the current profile, so that a log fit may not produce accurate estimates of u_{*c} and z_{0c} [Glenn and Grant, 1987; Friedrichs and Wright, 1997]. The major sources of stratification in the near-bed region at LEO-15 are temperature, salinity and suspended sediment. A vertical thermistor array located near the tripod measured no significant vertical temperature variations during the course of the deployment. The average temperature recorded by the BASS between year day 240 and 255 was 23.8C, with a standard deviation of 0.22C. Cross-shelf CTD transects conducted on year day 233 and 249 revealed no significant vertical salinity gradients. The average value for both of these transects at the tripod location was 31.8 ppt. The salinity recorded by the BASS between year day 240 and 255 had a mean value of 31.7 ppt with a standard deviation of 0.1 ppt. The potential effects of stratification due to suspended sediments were investigated for each burst by estimating the maximum stability parameter [Styles and Glenn, 2000] using Traykovski *et al.*'s [1999] suspended sediment concentration profile measurements to define the reference concentration. The maximum stability parameter is also a function of the time average and combined wave and current shear velocities. Time average values were obtained from the log profile fits and maximum combined shear velocities were obtained by running the neutral version of the Styles and Glenn [2000] BBLM with the wave and current parameters discussed above as input. For the 16 bursts, the results indicated a maximum stability parameter of 0.187 and a much lower mean of 0.018. Such low values have been shown theoretically to produce a negligible correction to current profile and shear stress estimates [Styles and Glenn, 2000] for conditions similar to those associated with the selected bursts.

4. Field Estimates for k_b

[15] Because the total bottom shear stress was not measured during the 1995 field effort, k_b is obtained with the aid of a combined wave and current bottom boundary layer model. The model used here is an extension of the Grant and Madsen [1979] BBLM, in which their 2-layer discontinuous eddy viscosity is replaced by a 3-layer continuous formulation [Madsen and Wikramanayake, 1991; Styles and Glenn, 2000]. For all calculations, we adopt the version presented by Styles and Glenn [2000] but without the correction for suspended sediment-induced stratification for reasons discussed above. The solution algorithm presented by Styles and Glenn [2000] assumes that k_b is given and the shear stresses are unknown. Relatively straightforward manipulation of the model equations shows that if u_{*c} and z_{0c} replace u_r and z_r as the input parameters, then z_0 ($= k_b/30$) rather than u_{*c} can be treated as an initially unknown parameter that is determined as part of the solution. A numerically efficient and stable algorithm is obtained by writing the equations in terms of the nondimensional input parameters u_{beq}/u_{*c} , φ_{cw} and A_{beq}/z_{0c} and the internal closure constant α , which defines the point at which the eddy viscosity in the wave boundary layer no longer increases with height [Madsen and Wikramanayake, 1991; Styles and Glenn, 2000]. Studies based on laboratory data have indicated that α ranges between about 0.15 and 0.5

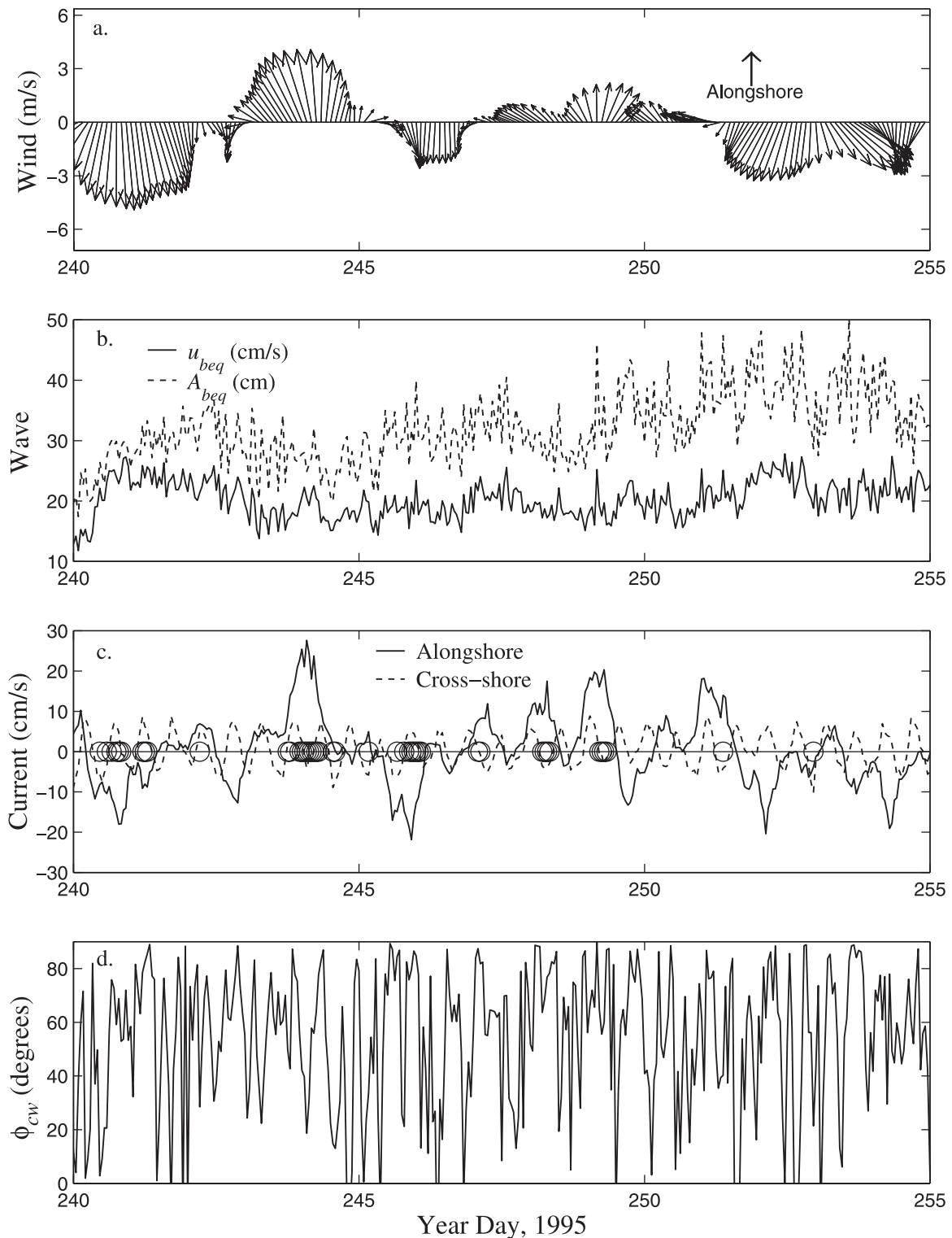


Figure 2. Wind, wave and current conditions for a 15-day period during the 1995 deployment. Forty-eight hour low-pass filtered wind vectors are obtained from NOAA buoy 44009 located offshore of Delaware Bay. Open circles on the current plot denote the 44 bursts that meet the data quality selection criteria to be included in the calibration data set.

[Madsen and Wikramanayake, 1991; Styles and Glenn, 2002].

[16] For each of the selected bursts, the model was run to produce an estimate of k_b . Because α remains a poorly

constrained parameter, each run was repeated with the following range: $\alpha = 0.15, 0.3$ and 0.5 . The average of the ratio k_b/η for all 44 bursts is listed in Table 1. The averages are much larger than the typical value of 4

Table 1. Bed Roughness Relationships as a Function of the Model Closure Constant α^a

α	k_b/η	$k_b \lambda/\eta^2$	k_b/η	$k_b \lambda/\eta^2$
0.15	20.3 \pm 3.6	121 \pm 23.3	9.8 \pm 1.3	58.5 \pm 8.8
0.30	20.2 \pm 3.6	121 \pm 23.4	6.4 \pm 0.9	38.2 \pm 5.9
0.50	18.6 \pm 3.9	111 \pm 25.1	4.3 \pm 0.7	25.7 \pm 4.4

^aThe second and third columns are computed without the enhancement to the eddy viscosity length scale, z_1 , as discussed in the text. The last two columns are computed with the enhancement. Confidence limits represent the 90% level of significance based on the sample variance [Bendat and Piersol, 1986].

obtained from detailed laboratory studies over rippled sand beds with a similar geometry as the orbital scale ripples found at LEO-15 [Wikramanayake and Madsen, 1991; Rankin and Hires, 2000]. Both Nielsen [1981] and Wikramanayake and Madsen [1991] have noted that irregular waves tend to produce ripples with slightly smaller steepnesses and that are more round crested than ripples formed by regular waves. For models that relate bottom roughness to ripple height, the roughness felt by irregular waves should be equal to or smaller than for regular waves. It is unexpected that the roughness for the LEO-15 data set, which is for irregular waves, has a much higher roughness than established formulations for regular waves. One obvious reason why the results might be different is that at LEO-15 the superposition of a steady current that flows obliquely to the direction of the wave can alter the roughness of an otherwise pure wave or pure current. Roughness models that include a correction to account for the direction between the wave and current [Sorenson *et al.*, 1995; Drake *et al.*, 1992] predict a decrease in the roughness for the current with increasing φ_{cw} . For 66% of all the bursts, φ_{cw} was greater than 45 degrees. On the basis of this argument, it is expected that the results for the wave-dominated conditions found at LEO-15 should produce an overall current roughness that is lower than the roughness associated with similar bedform geometry under a pure wave. This is not the case. Another possibility is that the BBLM, which is needed to compute the maximum wave shear stress and associated bottom roughness, is not properly calibrated for the range of conditions encountered at LEO-15 during the 1995 field study.

[17] Styles and Glenn [2002] determined that their version of the Grant and Madsen [1979] combined flow model was not very accurate at predicting friction factors and wave boundary layer thicknesses for very rough conditions. A plot depicting their theoretical friction factor curve as a function of A_{beq}/k_b for the 44 bursts is shown in Figure 3. The relative roughness, k_b/A_{beq} , for the majority of the calibration data set is greater than 1, indicating very rough conditions. On the basis of the combined flow data presented by Mathisen and Madsen [1996], Styles and Glenn [2002] hypothesized that for very rough conditions there is an enhancement to the turbulent transport associated with vortex ejection that increases the wave boundary layer thickness that is not accurately predicted by either the Styles and Glenn [2000] version or the original Grant and Madsen [1979] wave/current models. A very simple correction was implemented in which the scale height, z_1 ($=\alpha l_{cw}$), defining the transition layer in the eddy viscosity profile, was

modified as $z_1 = \alpha l_{cw}(1 + \beta k_b/A_{beq})$, where β is another internal closure constant, l_{cw} ($=\kappa u_{*cw}/\omega_{eq}$) is the scale height of the wave boundary layer, and u_{*cw} is the maximum shear stress for combined flows. Both α and β were calibrated using Mathisen and Madsen's [1996] laboratory flume data with co-directional waves and currents over artificial roughness elements that were scaled to approximate the geometry of 2-D wave-generated ripples. Optimum values ($\alpha = 0.3$ and $\beta = 0.7$) were determined by minimizing the variance between modeled and measured friction factors and the wave boundary layer thickness. The bottom roughness calculation is repeated with z_1 modified as described above. The results are listed in Table 1. In this case the average of k_b/η is much lower for a given α and shows closer agreement to roughnesses obtained for pure waves.

[18] To determine if the average is representative of the roughness for all the bursts, the Styles and Glenn [2002] version of the BBLM, which requires u_r and z_r as input parameters, was run using the formulations listed in Table 1 to compute k_b . The time average shear stress and apparent roughness are computed as part of the solution with their model, so that a comparison can be made with the measured values from the regression analysis. The parameter α is set with the two values, 0.3 and 0.5. The former is based on the recent calibration of Styles and Glenn [2002], who showed good comparisons for the wave friction factor and boundary layer thickness, and the latter is based on the results of Madsen and Wikramanayake [1991], who showed good agreement between measured and modeled current profiles. The results are presented in Figure 4 and are sorted in terms of increasing u_{*c} . The overall agreement is better for the modified version, especially for the largest values in which the unmodified model significantly over predicts the measurements. The agreement is improved for the unmodified version when $\alpha = 0.5$. However, the modified version is about equally accurate for both cases. Bottom roughness

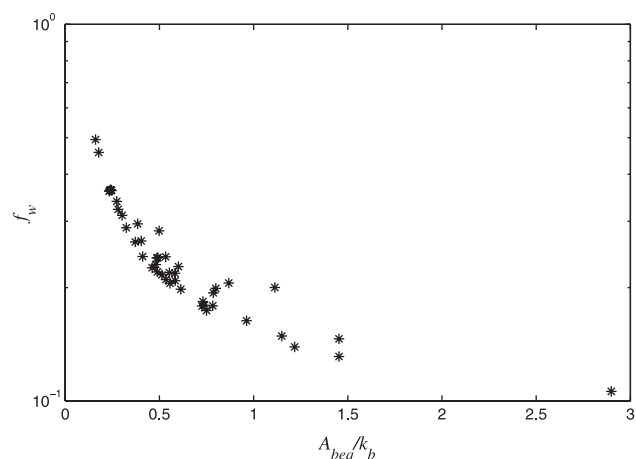


Figure 3. Theoretical friction factor curves as a function of A_{beq}/k_b , where k_b is the estimated bottom roughness obtained from running the Styles and Glenn [2000] model with u_{*c} and z_{0c} obtained from the regression analysis. Note that the curve is not smooth since the wave friction factor in combined flows is also a function of the current shear stress [Styles and Glenn, 2000].

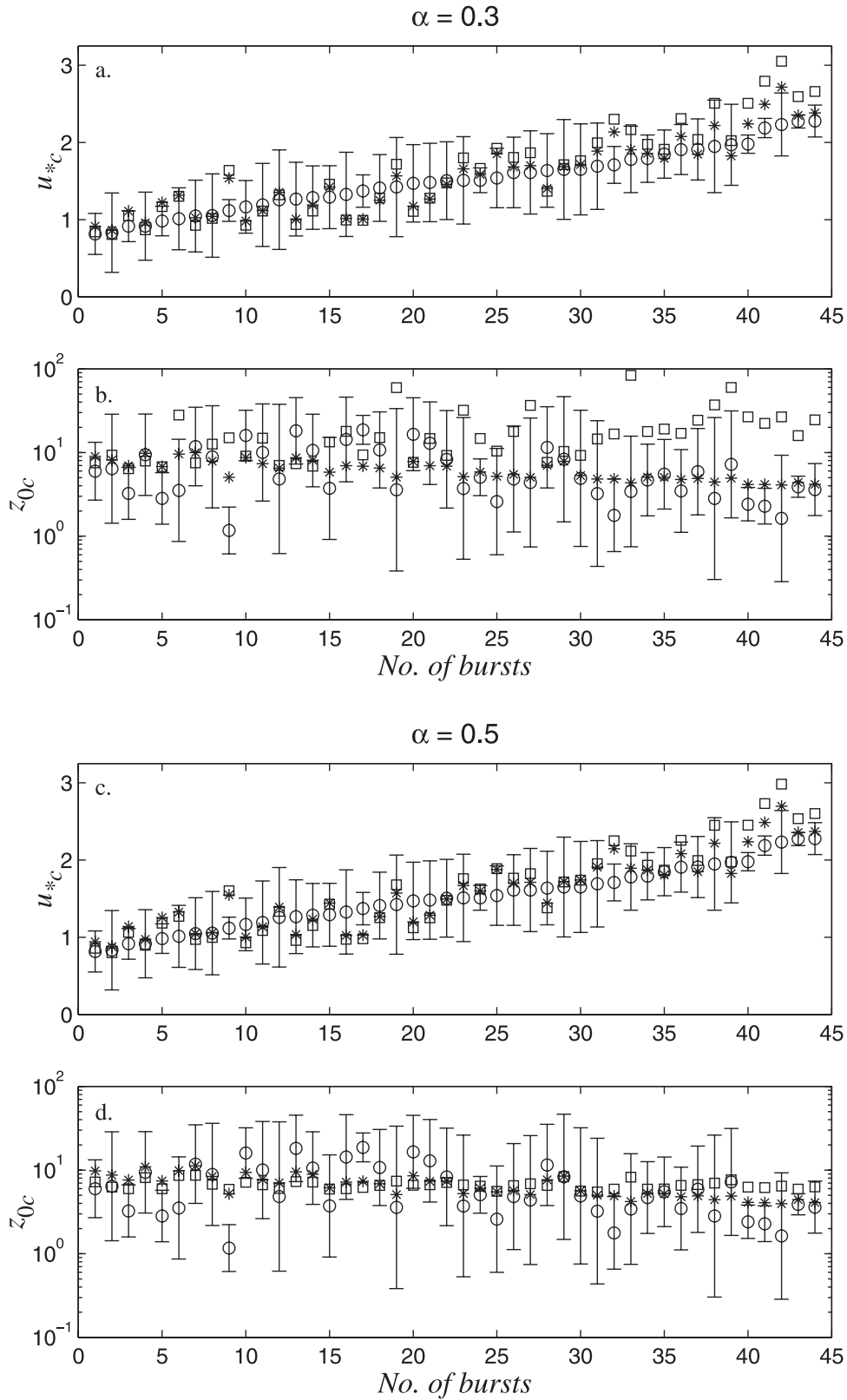


Figure 4. Measured and modeled time average shear stress and apparent roughness for the 44 bursts chosen from the 1995 LEO-15 deployment. (a) Comparison of measured (open circles), unmodified model (squares) and modified model (asterisks) sorted in terms of increasing u_{*c} . (b) Comparison of apparent roughness corresponding to u_{*c} in (a). (c) and (d), same as (a) and (b) but for $\alpha = 0.5$. Error bars denote 95% level of significance.

estimates were also obtained using the *Sorenson et al.* [1995] and *Drake et al.* [1992] models that include a correction to account for the angle between the wave and current. Although not shown, the modified model presented above still showed better agreement with the measurements.

[19] The above results are based on a semi-empirical approach in which the bottom roughness is obtained with the aid of a model. This is evident by the fact that the proportionality constant relating k_b to η is a function of the internal model closure constants α and β . It is emphasized that the results derived here are only valid as long as they are used in conjunction with the family of W. D. Grant, O. S. Madsen and S. M. Glenn [*Grant and Madsen*, 1979, 1986; *Glenn and Grant*, 1987] BBLMs, but modified with a 3-layer continuous eddy viscosity and the enhancement to z_1 as described by *Styles and Glenn* [2002].

5. Models of Wave-Generated Ripples

[20] Application of the roughness model to cases where the bedforms are not measured requires reliable estimates of ripple height. The geometrical characteristics of sand ripples generated under an oscillatory flow and how they respond to varying flow intensities have been studied extensively in the past [*Inman*, 1957; *Kennedy and Falcon*, 1965; *Carstens et al.*, 1969; *Mogridge and Kamphuis*, 1972; *Dingler*, 1974; *Miller and Komar*, 1980a, 1980b; *Nielsen*, 1981]. This has produced a wealth of data on ripple geometry for oscillatory flow that has led to the development of a number of competing ripple geometry models [*Nielsen*, 1981; *Grant and Madsen*, 1982; *Wikramanayake and Madsen*, 1991; *Mogridge et al.*, 1994; *Wiberg and Harris*, 1994; *Li et al.*, 1996; *Traykovski et al.*, 1999]. *Wiberg and Harris* [1994], using data sets obtained from both field [*Inman*, 1957; *Dingler*, 1974] and laboratory [*Carstens et al.*, 1969; *Kennedy and Falcon*, 1965; *Mogridge and Kamphuis*, 1972; *Dingler*, 1974] studies, concluded that for orbital scale ripples, which approximately correspond to equilibrium ripples, λ scaled with the wave orbital diameter, d_0 , ($\lambda = 0.62d_0$, where $d_0 = 2A_b$) and ripple steepness was constant ($\eta/\lambda = 0.17$). For the field data, *Wiberg and Harris* [1994] used the significant wave height to compute d_0 . *Traykovski et al.* [1999] obtained similar results for ripples they measured at LEO-15 using an SSS, but with different values for the constants, $\lambda = 0.75d_0$ and $\eta/\lambda = 0.15$. Under stronger flows, *Wiberg and Harris* [1994] noted that ripple length was proportional to grain size ($\lambda = 535d$) and ripple steepness decreased with increasing flow intensity. On the basis of the available data, they developed a parametric model that related ripple steepness to d_0 under these conditions. Their analysis resulted in an accurate ripple geometry model valid for a broad range of flow and sediment conditions, with wave orbital diameter and sediment grain size the only input parameters. *Wiberg and Harris* [1994] noted that their model may be less efficient when used to produce a time series of ripple height and length, since under certain combinations of wave and sediment conditions, their equation for ripple steepness was transcendental and had to be solved iteratively. A similar situation may arise when their ripple model is applied as a subroutine in a circulation model, where the ripple geometry algorithm would be implemented many times during a simulation.

An empirical ripple model that is written explicitly as a function of the independent input parameters for its full range of validity is probably more efficient, although it should be noted that for orbital scale ripples, the *Wiberg and Harris* [1994] formulation is much simpler to use and is the preferred method under these conditions.

[21] *Wikramanayake and Madsen* [1991] reviewed several nondimensional parameters commonly used in sediment transport studies and found that the ratio of the mobility number,

$$\theta_m = \frac{(A_{brms}\omega)^2}{(s-1)gd} \quad (4)$$

to the nondimensional sediment parameter,

$$S_* = \frac{d}{4\nu}[(s-1)gd]^{1/2} \quad (5)$$

was well correlated with the field ripple data of *Inman* [1957], *Dingler* [1974] and *Nielsen* [1984]. Plotting relative ripple height (η/A_{brms}) and relative ripple length (λ/A_{brms}) as a function of this ratio produced the following empirical relationship to predict η and λ ,

$$\frac{\eta}{A_{brms}} = \begin{cases} 0.27 X^{-0.5} & X \leq 3 \\ 0.52 X^{-1.1} & X \geq 3 \end{cases}, \quad (6)$$

$$\frac{\lambda}{A_{brms}} = \begin{cases} 1.7 X^{-0.5} & X \leq 3 \\ 2.1 X^{-0.7} & X \geq 3 \end{cases},$$

where the nondimensional wave and sediment parameter, X , is defined by

$$X = \frac{\theta_m}{S_*} = \frac{4\nu(A_{brms}\omega)^2}{d[(s-1)gd]^{1.5}} \quad (7)$$

and A_{brms} is the root-mean square bottom excursion amplitude, ν is the kinematic viscosity of the water, s is the ratio of the sediment density, ρ_s , to the fluid density, ρ , and g is the acceleration due to gravity. For $X < 3$, the -0.5 exponent for X results in expressions for η and λ that are independent of water depth and the bottom excursion amplitude, A_b , and become functions only of the wave period. This is a physically unreasonable result for the continental shelf under equilibrium conditions when the ripples are known to scale with A_b . Moreover, the fitting parameters will vary depending on how A_b is calculated. As a result, η/A_b and λ/A_b are recalculated using the field data obtained by *Traykovski et al.* [1999] at LEO-15, the data originally used by *Wikramanayake and Madsen* [1991] to obtain (6), and the field data used by *Wiberg and Harris* [1994].

[22] *Wikramanayake and Madsen* [1991] and *Wiberg and Harris* [1994] used the field data of *Inman* [1957] and *Dingler* [1974], and *Wikramanayake and Madsen* [1991] also used the data of *Nielsen* [1984]. Each of these investigators reported sediment grain size, ripple height, ripple length, wave period and wave height or orbital velocity, and *Dingler* [1974] and *Nielsen* [1984] also recorded water temperature. *Wikramanayake and Madsen* [1991] converted

the originally measured wave heights to A_{brms} . The equivalent near-bottom orbital amplitude, A_{beq} , is easily obtained from A_{brms} since $A_{beq} = \sqrt{2} A_{brms}$. This, along with ω and the sediment and fluid parameters reported by *Wikramanayake and Madsen* [1991], are used to compute the coefficients of X.

[23] The method to determine the error associated with the best fit is adopted from *Wikramanayake and Madsen* [1991] who used the relative error defined by

$$\ln(e) = \left[\frac{1}{N} \sum_{i=1}^N (\ln(Y_i) - \ln(\bar{Y}_i))^2 \right]^{1/2}, \quad (8)$$

where Y_i is the measured data point, \bar{Y}_i is the corresponding model estimate and N is the number of observations. As noted by *Wikramanayake and Madsen* [1991], when e is minimized, (8) is a least squares fit on a log-log plot. As part of the recalibration, the break point $X = 3$ determined by *Wikramanayake and Madsen* [1991] was varied between a maximum of 5 and a minimum of 0.5. The value that produced the lowest e was designated the new break point. The results of the recalibration are depicted in Figure 5.

[24] Noticeable is the natural extension of the *Traykovski et al.* [1999] data set into the smaller range of X where the original field data used by *Wikramanayake and Madsen* [1991] and *Wiberg and Harris* [1994] are more scarce. A natural break point of $X = 2$ for both η/A_{beq} and λ/A_{beq} gives the lowest overall e with values of 1.33 and 1.25, respectively. Equivalent errors calculated by *Wikramanayake and Madsen* [1991] for $X = 3$ are 1.88 for η/A_{brms} and 1.75 for λ/A_{brms} . The refined coefficients associated with the best fit curves are given by,

$$\frac{\eta}{A_{beq}} = \begin{cases} 0.30 X^{-0.39} & X \leq 2 \\ 0.45 X^{-0.99} & X \geq 2 \end{cases}, \quad (9)$$

$$\frac{\lambda}{A_{beq}} = \begin{cases} 1.96 X^{-0.28} & X \leq 2 \\ 2.71 X^{-0.75} & X \geq 2 \end{cases}.$$

Because none of the exponents are -0.5 , η and λ remain functions of A_{beq} as expected. The results shown in Figure 5 further indicate that (9) is valid in the range $0.1 < X < 100$. For $X > 2$, η decays at a rate nearly proportional to $1/A_{beq}$. This is qualitatively consistent with the measured behavior of wave-generated ripples for conditions beyond the equilibrium range, where η no longer increases in proportion to A_{beq} but begins to decay with increasing wave energy. It should be noted that while *Wikramanayake and Madsen* [1991] used A_{brms} , our choice to use the larger equivalent orbital amplitude effectively shifts the data to the left along the X axis. This is in part why we obtain the lowest errors with a smaller break point, and emphasizes the fact that the ripple model is sensitive to the definition of A_b .

[25] A comparison of the ripple measurements of *Traykovski et al.* [1999] and (9) are depicted in Figure 6. Ripple geometry predictions using the *Wiberg and Harris* [1994] model have been discussed by *Traykovski et al.* [1999] and are very similar to the results presented here. The shaded

areas denote *Traykovski et al.*'s [1999] periods of hysteresis or 3-D ripples. Equation (9), which assumes 2-D ripples that are in equilibrium with the waves, may not apply during these times. Although this is not an independent test of (9), the results indicate that natural ripples exhibit characteristics that are well described by this simple model formulation.

6. Evaluation of the Combined Ripple/Roughness Model

[26] The predictive capabilities of the combined ripple geometry/bottom roughness model are assessed using storm data collected during the 1994 deployment. Only the near-bottom flow and wave parameters were measured so that the bottom roughness and ripple geometry are obtained from the models presented above. Unlike the calibration, the input parameters revert back to u_r and z_r so that u_{*c} and z_{0c} are computed as part of the solution [*Styles and Glenn*, 2000]. The accuracy of the refined ripple geometry/roughness model is assessed through a comparison of u_{*c} and z_{0c} obtained from the BBLM and the results obtained from log profile fits to the BASS data. Figure 7 shows the measured wave and current, and the computed ripple height and Shields parameter time series bracketing a moderate north-easter captured during the 1994 LEO-15 deployment. The magnitude of the Shields parameter based on skin friction was calculated as

$$\Psi_w' = \frac{\tau_{wm}'}{\rho(s-1)gd}, \quad (10)$$

where τ_{wm}' is the maximum shear stress based on skin friction for the wave. The stress is computed using a modification to the equivalent wave velocity [*Traykovski et al.*, 1999] from each burst,

$$\frac{\tau_{wm}'}{\rho} = \frac{f_w}{2} (\sqrt{2}u_{beq})^2 \quad (11)$$

and the friction factor [*Madsen*, 1994] is determined using the burst estimate of A_{beq} , i.e.,

$$f_w = \exp \left[5.61 \left(\frac{A_{beq}}{d} \right)^{-0.109} - 7.3 \right]. \quad (12)$$

Before the storm, waves are directed onshore and the currents are dominated by tides. As the storm intensifies, the waves and currents align themselves with the coast and increase significantly to peak values of 37 and 44 cm/s, respectively. As the storm passes, the currents are reduced quickly while the waves remain fairly large. Estimates of the wave-induced skin friction Shields parameter (Figure 7b) indicate sediment resuspension during the storm and for about a day afterwards. Since the measured wave conditions favor the mobilization of bed sediments, the ripple model can be applied to predict η and λ . Modeled ripple height (Figure 7c) initially grows as the storm intensifies, but then begins to decrease during the maximum waves. By the end of the storm, η has again increased. The decay in η during the most intense portion of the storm is accompanied by a

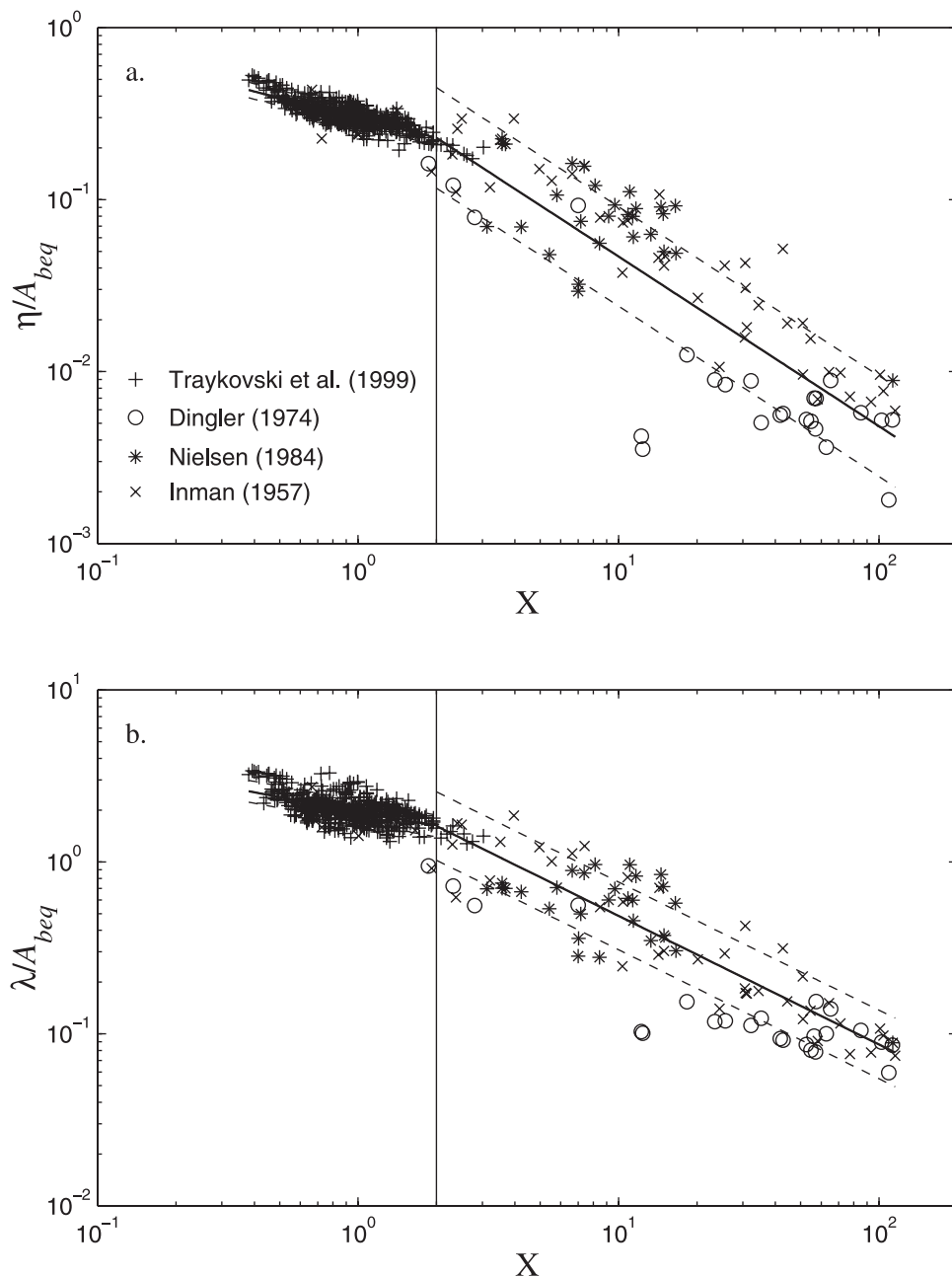


Figure 5. Relative ripple height (a) and length (b) as a function of the nondimensional wave and sediment parameter, X . Solid line denotes best fit curve. Dashed line denotes one standard deviation.

decrease in ripple steepness suggesting that the ripples are starting to washout. Modeled ripple height never decreases below 7 cm during the storm so that it is unlikely that a complete transition to sheet flow took place; although the results provide evidence that the initial stages did occur. Because it appears as if the ripples remained fairly close to a state of equilibrium, this storm provides an excellent test case for the refined ripple roughness model.

[27] A comparison between measured and modeled u_{*c} and z_{0c} for $\alpha = 0.3$ and 0.5 during the most intense portion of storm are shown in Figure 8. Also shown are the results obtained without the correction to z_1 . The shear stress and apparent roughness are accurately predicted with the refined ripple geometry/bottom roughness model during the majority

of the storm, especially for the most intense period between hour 8 and 13. Considering that the overall range of u_{*c} is higher than the 44 calibration bursts from the 1995 data set, the modified model maintains its accuracy during these stronger conditions. The uncorrected model significantly over predicts the shear stress near the storm peak when $\alpha = 0.5$, but it is more accurate when $\alpha = 0.3$. This is opposite to the calibration results depicted in Figure 4, where the uncorrected model was more accurate for the larger value of α . Between hour 4 and 7, all models consistently over predict u_{*c} and z_{0c} . Examination of the original time series indicates that during this 4 hour interval, one of the tripod legs is directly upstream of the BASS sensor cages with respect to the mean horizontal flow. This places the lower 3 BASS sensors in the

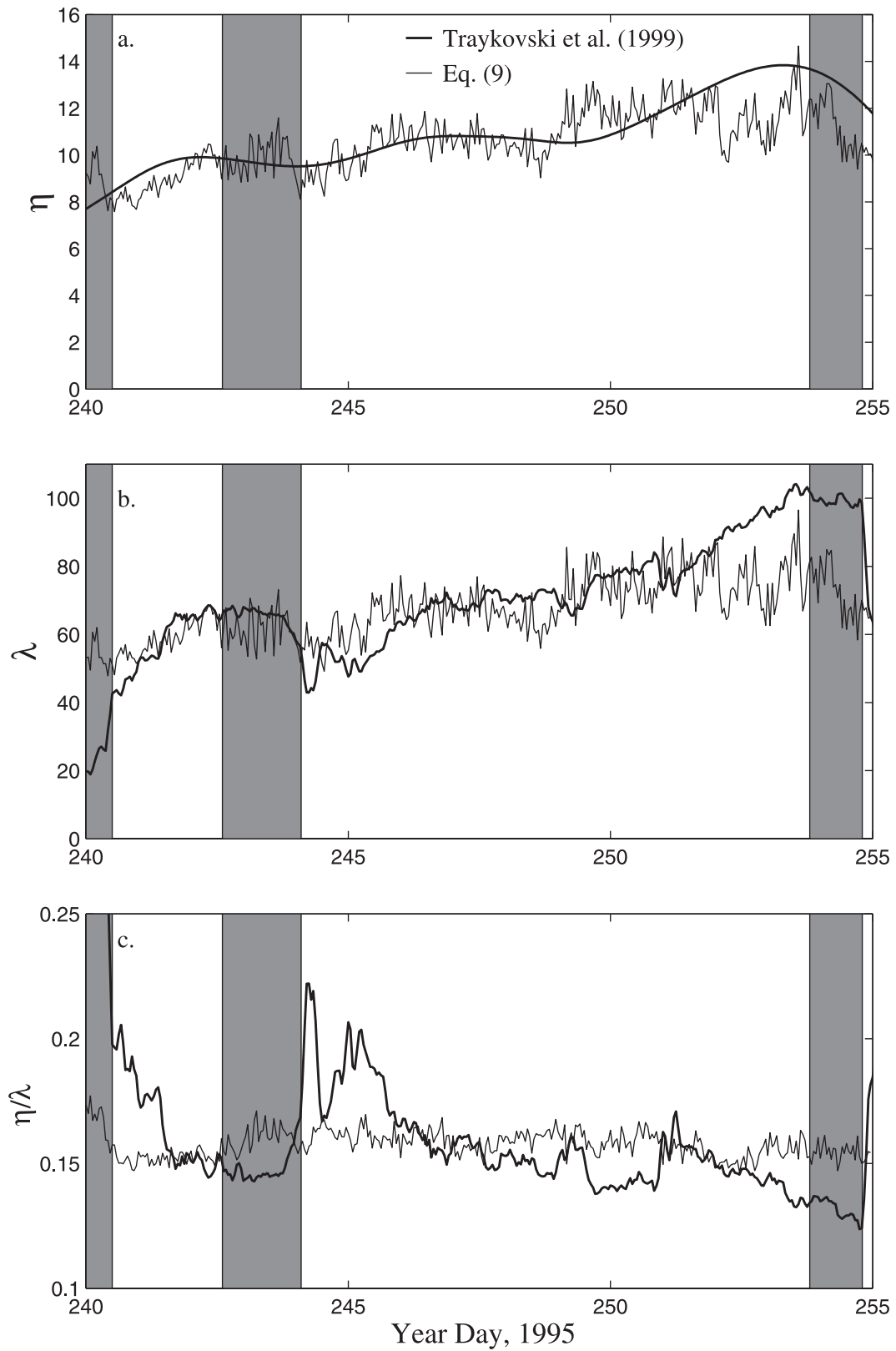


Figure 6. Comparison of η , λ and η/λ obtained from the best fit curve computed from (9) and the *Traykovski et al.* [1999] ripple geometry data. Shaded areas denote *Traykovski et al.*'s [1999] periods of 3-D ripples or hysteresis.

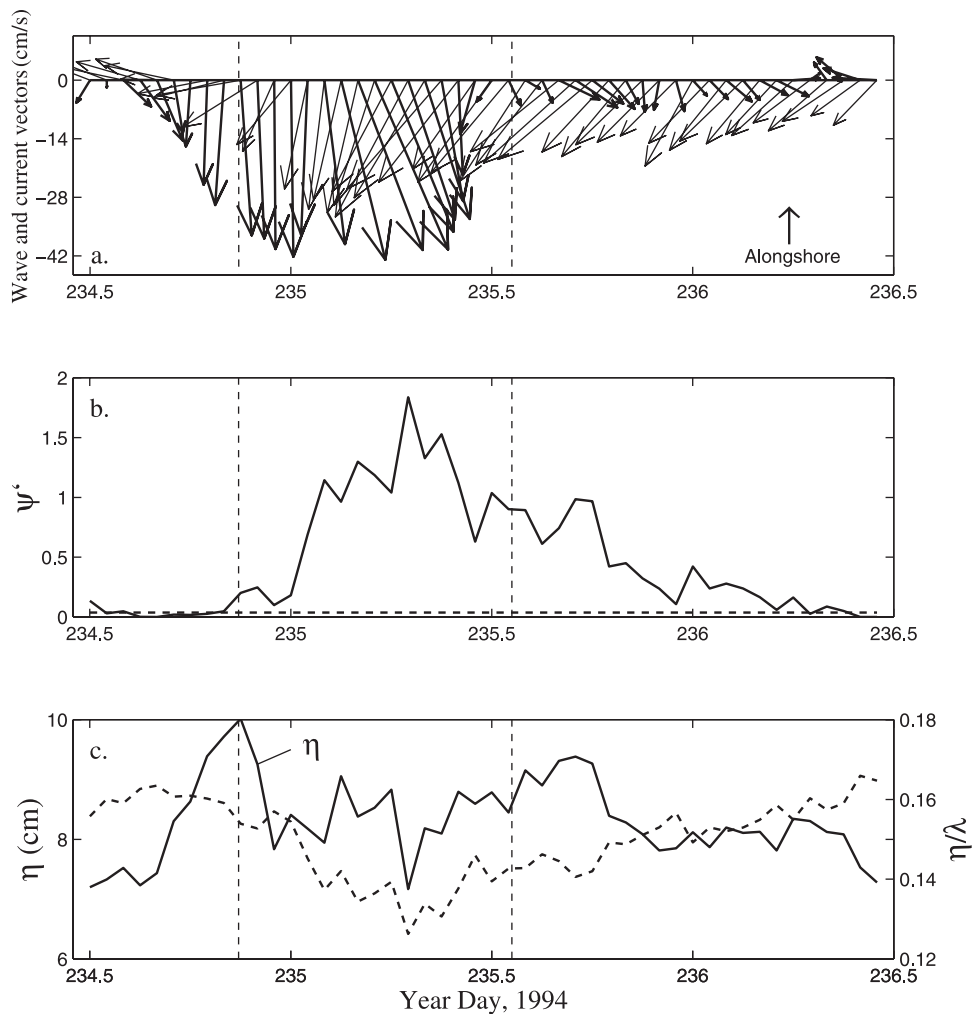


Figure 7. Measured wave and current conditions, along with selected sediment transport parameters, bracketing a moderate northeaster during the 1994 deployment. (a) Wave (thin) and current (thick) vectors, (b) burst-averaged (solid) and critical (dashed) Shields parameter based on skin friction, and (c) ripple height and ripple steepness. The vertical dashed lines identify the boundaries of the most severe segment of the storm (see Figure 8).

path of the turbulent wake induced by the tripod leg. Assuming the flow pattern in the wake of the tripod leg behaves similarly to the flow around a circular cylinder [Hinze, 1975], it is likely that the current measured by the BASS is reduced. This reduces the shear and produces lower values of u_{*c} and z_{0c} , which is consistent with the observations.

7. Conclusions

[28] High-quality current, wave and ripple geometry measurements were collected at the sandy LEO-15 site located off of the southern coast of New Jersey. The measurements were used to refine empirical coefficients identified with existing bottom roughness and ripple geometry formulations. The physical bottom roughness associated with nearly 2-D wave-generated ripples was determined to be well represented as a constant times the height of the ripples. Because the total bed shear stress was not measured, the roughness was computed with the aid of a BBLM. It was emphasized that the empirically derived proportionality constant relating k_b to ripple height was

only valid when used in conjunction with the *Styles and Glenn* [2002] version of the *Grant and Madsen* [1979] combined flow model. In particular, a modification to the eddy viscosity profile was introduced that produced an additional closure constant that is absent from the *Grant and Madsen* [1979] model. On the basis of previous calibrations [Styles and Glenn, 2002] and the improved agreement between modeled and measured shear stress and apparent roughness shown here, the following values are suggested for use in applications $\alpha = 0.5$ and $\beta = 0.7$.

[29] Ripple geometry and wave data collected using an SSS and BASS, respectively, were used to further refine estimates of the fitting parameters associated with the *Wikramanayake and Madsen* [1991] ripple geometry model. The recalibrated ripple height and length equations showed lower relative errors than the original calibration conducted by *Wikramanayake and Madsen* [1991] and appeared to produce accurate results for equilibrium conditions, when η and λ scale with A_b . It was emphasized that the numerical value of the fitting parameters are sensitive to the definition of A_b . For the refined model presented here, the equivalent

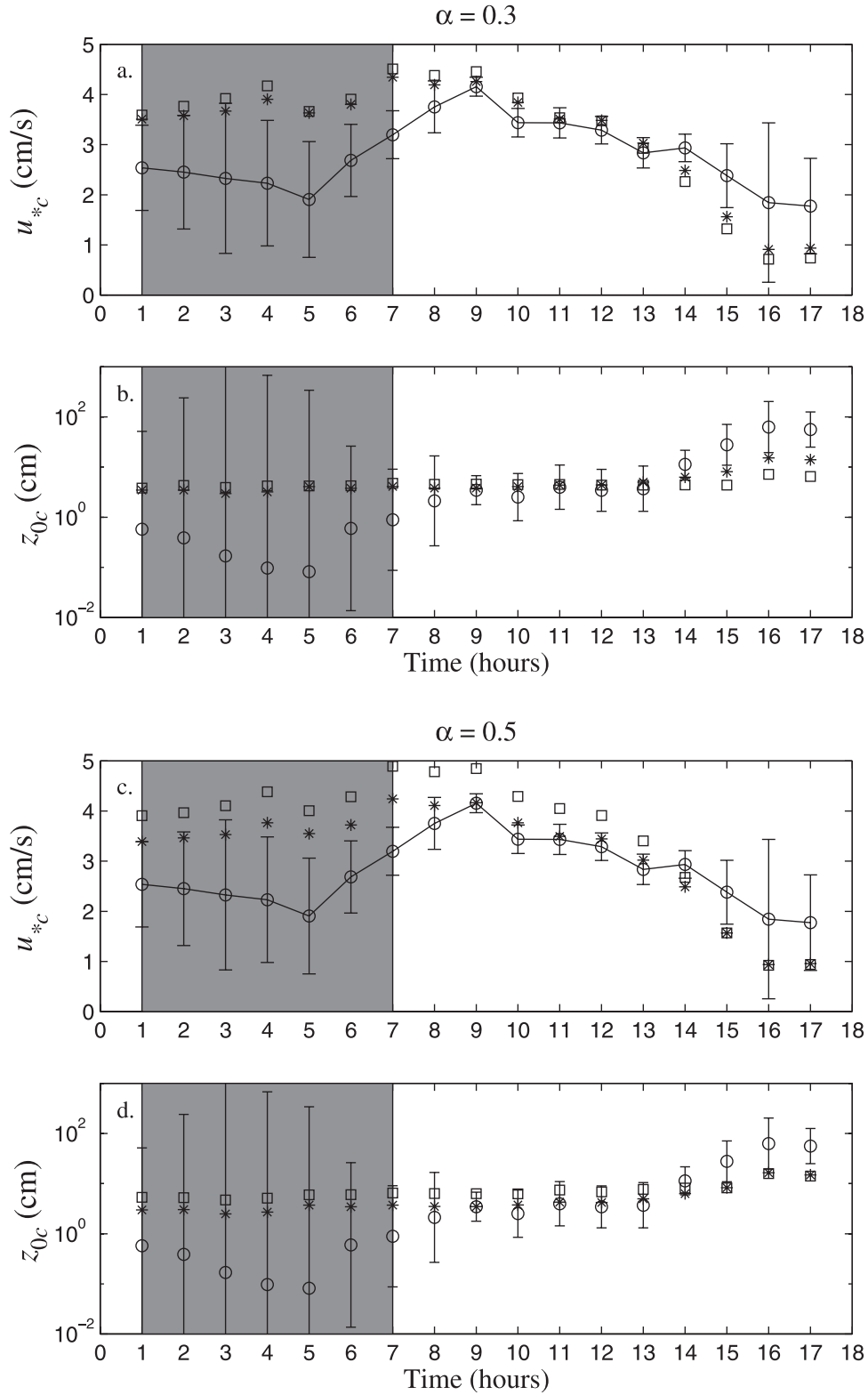


Figure 8. Comparison of measured and modeled u_{*c} and z_{0c} during the most severe segment of the storm. (a) Measured (open circles) and modeled u_{*c} with the modification to α (asterisks) and without the modification (squares). (b) Same as (a) for z_{0c} . (c) and (d), same as (a) and (b), but for $\alpha = 0.5$. Shaded area identifies a period when the mean flow around the lower 3 BASS sensor pods experiences interference from an upstream tripod leg.

wave parameters defined in (1) and (2) should always be used in ripple geometry calculations. A quantitative assessment of the refined bottom roughness/ripple geometry model showed that, when used in conjunction with the *Styles and Glenn* [2002] version of the *Grant and Madsen* [1979] BBLM, it produced accurate estimates of the time averaged shear stress and apparent roughness during a moderate northeaster.

[30] **Acknowledgments.** The authors would like to thank James Irish, James Lynch and Peter Traykovski of the Woods Hole Oceanographic Institution for providing the concentration and ripple data. The first author was supported through the Office of Naval Research/Augmentation Awards in Science and Engineering Research Training (ONR/AASERT) under grant 4-26420. The second author was supported by ONR/COMOP (Coastal Ocean Modeling and Observation Program) under grant N00014-97-1-0797. Both authors acknowledge the continued support of the National Oceanographic and Atmospheric Administration/National Undersea Research Program (NOAA/NURP) under grants MAB 96-10, NYB 94-7 and NA06RU0139, the National Science Foundation (OCE-95-21102), and the National Ocean Partnership Program (N00014-97-1-1019 and N00014-98-1-0815).

References

- Bagnold, R. A., Motion of waves in shallow water: Interaction of waves and sand bottom, *Proc. R. Soc. London, Ser. A*, 187, 1–15, 1946.
- Bagnold, R. A., Flow of cohesionless grains in fluids, *Philos. Trans. R. Soc. London, Ser. A*, 249, 235–297, 1956.
- Bendat, J. S., and A. G. Piersol, *Random Data, Analysis and Measurement Procedures*, 566 pp., Wiley-Interscience, New York, 1986.
- Blackadar, A. K., and H. Tennekes, Asymptotic similarity in neutral barotropic planetary boundary layers, *J. Atmos. Sci.*, 25, 1015–1020, 1968.
- Carstens, M. R., F. M. Neilson, and H. D. Altinbilek, Bed forms generated in the laboratory under an oscillatory flow: Analytical and experimental study, *Tech. Memo. 28*, 39 pp., Coastal Eng. Res. Cent., U.S. Corps of Eng., Washington, D. C., 1969.
- Davies, A. G., R. L. Soulsby, and H. L. King, A numerical model of the combined wave and current bottom boundary layer, *J. Geophys. Res.*, 93, 491–508, 1988.
- Dingler, J. R., Wave-formed ripples in nearshore sands, Ph.D. thesis, Univ. of Calif., San Diego, 1974.
- Drake, D. E., and D. A. Cacchione, Wave-current interaction in the bottom boundary layer during storm and non-storm conditions: observations and model predictions, *Cont. Shelf Res.*, 12, 1331–1352, 1992.
- Drake, D. E., D. A. Cacchione, and W. D. Grant, Shear stress and bed roughness estimates for combined wave and current flows over a rippled bed, *J. Geophys. Res.*, 97, 2319–2326, 1992.
- Friedrichs, C. T., and L. D. Wright, Sensitivity of bottom stress and bottom roughness estimates to density stratification, Eckernforde Bay, southern Baltic Sea, *J. Geophys. Res.*, 102, 5721–5732, 1997.
- Glenn, S. M., and W. D. Grant, A suspended sediment correction for combined wave and current flows, *J. Geophys. Res.*, 92, 8244–8246, 1987.
- Glenn, S. M., T. D. Dickey, B. Parker, and W. Boicourt, Long-term real-time coastal ocean observation networks, *Oceanography*, 13, 24–34, 2000.
- Grant, W. D., and O. S. Madsen, Combined wave and current interaction with a rough bottom, *J. Geophys. Res.*, 84, 1797–1808, 1979.
- Grant, W. D., and O. S. Madsen, Movable bed roughness in unsteady oscillatory flow, *J. Geophys. Res.*, 87, 469–481, 1982.
- Grant, W. D., and O. S. Madsen, The continental-shelf bottom boundary layer, *Annu. Rev. Fluid Mech.*, 18, 265–305, 1986.
- Gross, T. F., and A. R. M. Nowell, Mean flow and turbulence scaling in a tidal boundary layer, *Cont. Shelf Res.*, 2, 109–126, 1983.
- Gross, T. F., A. E. Isley, and C. R. Sherwood, Estimation of stress and bed roughness during storms on the Northern California shelf, *Cont. Shelf Res.*, 12, 389–413, 1992.
- Gross, T. F., A. J. Williams, and E. A. Terray, Bottom boundary layer spectral dissipation estimates in the presence of wave motions, *Cont. Shelf Res.*, 14, 1239–1256, 1994.
- Hay, A. E., and D. J. Wilson, Rotary side scan images of near-shore bed-form evolution during a storm, *Mar. Geol.*, 119, 57–65, 1994.
- Hinze, J. O., *Turbulence*, 790 pp., McGraw-Hill, New York, 1975.
- Inman, D. L., Wave generated ripples in nearshore sands, *Tech. Memo. 100*, 66 pp., Beach Erosion Board, U.S. Army Corps of Eng., Washington, D. C., 1957.
- Kennedy, J. F., and M. Falcon, Wave generated sediment ripples, *Rep. 86*, Hydrodyn. Lab., Mass. Inst. of Technol., Cambridge, 1965.
- Komar, P. D., and M. C. Miller, The initiation of oscillatory ripple marks and the development of plane-bed at high shear stresses under waves, *J. Sediment. Petrol.*, 45, 697–703, 1975.
- Li, M. Z., and C. L. Amos, Predicting ripple geometry and bed roughness under combined waves and currents in a continental shelf environment, *Cont. Shelf Res.*, 18, 941–970, 1998.
- Li, M. Z., L. D. Wright, and C. L. Amos, Predicting ripple roughness and sand resuspension under combined flows in a shoreface environment, *Mar. Geol.*, 130, 139–161, 1996.
- Lofquist, K. E. B., Drag on natural rippled beds under oscillatory flows, *Misc. Pap. CERC-86-13*, 121 pp., U.S. Army Corps of Eng., Washington, D. C., 1986.
- Madsen, O. S., Spectral wave-current bottom boundary layer flows, paper presented at 24th Coastal Engineering Conference, Am. Soc. of Civ. Eng., Kobe, Japan, 1994.
- Madsen, O. S., and P. N. Wikramanayake, Simple models for turbulent wave-current bottom boundary layer flow, *Contract Rep. DRP-91-1*, 150 pp., Coastal Eng. Res. Cent., U.S. Army Corps of Eng., Washington, D. C., 1991.
- Madsen, O. S., Y.-K. Poon, and H. C. Graber, Spectral wave attenuation by bottom friction: Theory, paper presented at 21st Coastal Engineering Conference, Am. Soc. of Civ. Eng., Torremolinos, Spain, 1988.
- Madsen, O. S., L. D. Wright, J. D. Boon, and T. A. Chisholm, Wind stress, bed roughness and sediment suspension on the inner shelf during an extreme storm event, *Cont. Shelf Res.*, 13, 1303–1324, 1993.
- Mathisen, P. P., and O. S. Madsen, Waves and currents over a fixed rippled bed, 1, Bottom roughness experienced by waves in the presence and absence of currents, *J. Geophys. Res.*, 101, 16,533–16,542, 1996.
- Miller, M. C., and P. D. Komar, Oscillation sand ripples generated by laboratory apparatus, *J. Sediment. Petrol.*, 50, 173–182, 1980a.
- Miller, M. C., and P. D. Komar, A field investigation of the relationship between oscillation ripples spacing and the near-bottom water orbital motions, *J. Sediment. Petrol.*, 50, 183–191, 1980b.
- Mogridge, G. R., and J. W. Kamphuis, Experiments on bedform generation by wave action, paper presented at 13th Coastal Engineering Conference, Am. Soc. of Civ. Eng., Vancouver, 1972.
- Mogridge, G. R., M. H. Davies, and D. H. Willis, Geometry prediction for wave-generated bedforms, *Coastal Eng.*, 22, 255–286, 1994.
- Nielsen, P., Dynamics and geometry of wave-generated ripples, *J. Geophys. Res.*, 86, 6467–6472, 1981.
- Nielsen, P., Field measurements of time-averaged suspended sediment concentrations under waves, *Coastal Eng.*, 8, 51–72, 1984.
- Nielsen, P., *Coastal Bottom Boundary Layers and Sediment Transport*, 324 pp., World Sci., River Edge, N. J., 1992.
- Rankin, K. L., and R. I. Hires, Laboratory measurement of bottom shear stress on a movable bed, *J. Geophys. Res.*, 105, 17,011–17,019, 2000.
- Smith, J. D., Modeling of sediment transport on continental shelves, in *The Sea*, vol. 6, edited by E. D. Goldberg et al., pp. 538–577, Wiley-Interscience, New York, 1977.
- Smith, J. D., and S. R. McLean, Spatially averaged flow over a wavy surface, *J. Geophys. Res.*, 82, 1735–1746, 1977.
- Sorenson, K. S., O. S. Madsen, and L. D. Wright, Evidence of directional-dependence of moveable bottom roughness in inner shelf waters (abstract), *Eos Trans. AGU*, 76(46), Fall Meet. Suppl., F281, 1995.
- Styles, R., and S. M. Glenn, Modeling stratified wave and current bottom boundary layers on the continental shelf, *J. Geophys. Res.*, 105, 24,119–24,139, 2000.
- Styles, R., and S. M. Glenn, An optimized combined wave and current algorithm for arbitrary bed roughness, technical report, Coastal Phys. Oceanogr. Lab., Dep. of Geol. Sci., Univ. of S. C., Columbia, 2002.
- Tennekes, H., and J. L. Lumley, *A First Course in Turbulence*, 300 pp., MIT Press, Cambridge, Mass., 1972.
- Traykovski, P. A., E. Hay, J. D. Irish, and J. F. Lynch, Geometry, migration, and evolution of wave orbital ripples at LEO-15, *J. Geophys. Res.*, 104, 1505–1524, 1999.
- Trowbridge, J., On a technique for measurement of turbulent shear stress in the presence of surface waves, *J. Atmos. Oceanic Technol.*, 15, 290–298, 1998.
- von Alt, C. J., and J. F. Grassle, LEO-15: An unmanned long term environmental observatory, paper presented at Oceans 92, Inst. of Electr. and Electron. Eng., Newport, R. I., 1992.
- Wiberg, P., and C. K. Harris, Ripple geometry in wave-dominated environments, *J. Geophys. Res.*, 99, 775–789, 1994.
- Wiberg, P., and J. D. Smith, A comparison of field data and theoretical models for wave-current interactions at the bed on the continental shelf, *Cont. Shelf Res.*, 2, 147–162, 1983.

- Wikramanayake, P. N., and O. S. Madsen, Calculation of movable bed friction factors, *Tech. Rep. DACW-39-88-K-0047*, 105 pp., Coastal Eng. Res. Cent., U.S. Army Corps of Eng., Vicksburg, Miss., 1991.
- Williams, A. J., J. S. Tochko, R. L. Koehler, W. D. Grant, T. F. Gross, and C. V. R. Dunn, Measurements of turbulence in the ocean bottom boundary layer with an acoustic current meter array, *J. Atmos. Oceanic Technol.*, *4*, 312–327, 1987.
- Williams, J. J., C. P. Rose, P. D. Thorne, B. A. O'Connor, J. D. Humphery, P. J. Hardcastle, S. P. Moores, J. A. Cooke, and D. J. Wilson, Field observations and predictions of bed shear stresses and vertical suspended sediment concentration profiles in wave-current conditions, *Cont. Shelf Res.*, *19*, 507–536, 1999.
- Wilson, K. C., Friction of wave-induced sheet flow, *Coastal Eng.*, *12*, 371–379, 1989.
- Xu, J. P., and L. D. Wright, Tests of bed roughness models using field data from the Middle Atlantic Bight, *Cont. Shelf Res.*, *15*, 1409–1434, 1995.
-
- S. M. Glenn, Institute of Marine and Coastal Sciences, Rutgers University, 71 Dudley Road, New Brunswick, NJ 08901, USA. (glenn@caribbean.rutgers.edu)
- R. Styles, Department of Geological Sciences, University of South Carolina, 700 Sumter Street, Columbia, SC 29208, USA. (rstyles@geol.sc.edu)